AIP Physics of Plasmas

Integrated simulations of saturated neoclassical tearing modes in DIII-D, Joint European Torus, and ITER plasmas

Federico D. Halpern, Glenn Bateman, and Arnold H. Kritz

Citation: Phys. Plasmas 13, 062510 (2006); doi: 10.1063/1.2205829
View online: http://dx.doi.org/10.1063/1.2205829
View Table of Contents: http://pop.aip.org/resource/1/PHPAEN/v13/i6
Published by the AIP Publishing LLC.

Integrated simulations of saturated neoclassical tearing modes in DIII-D, Joint European Torus, and ITER plasmas

Federico D. Halpern, Glenn Bateman, and Arnold H. Kritz
Department of Physics, Lehigh University 16 Memorial Drive East, Bethlehem, Pennsylvania 18015

(Received 28 December 2005; accepted 26 April 2006; published online 19 June 2006)

A revised version of the ISLAND module [C. N. Nguyen *et al.*, Phys. Plasmas **11**, 3604 (2004)] is used in the BALDUR code [C. E. Singer *et al.*, Comput. Phys. Commun. **49**, 275 (1988)] to carry out integrated modeling simulations of DIII-D [J. Luxon, Nucl. Fusion **42**, 614 (2002)], Joint European Torus (JET) [P. H. Rebut *et al.*, Nucl. Fusion **25**, 1011 (1985)], and ITER [R. Aymar *et al.*, Plasma Phys. Control. Fusion **44**, 519 (2002)] tokamak discharges in order to investigate the adverse effects of multiple saturated magnetic islands driven by neoclassical tearing modes (NTMs). Simulations are carried out with a predictive model for the temperature and density pedestal at the edge of the high confinement mode (H-mode) plasma and with core transport described using the Multi-Mode model. The ISLAND module, which is used to compute magnetic island widths, includes the effects of an arbitrary aspect ratio and plasma cross sectional shape, the effect of the neoclassical bootstrap current, and the effect of the distortion in the shape of each magnetic island caused by the radial variation of the perturbed magnetic field. Radial transport is enhanced across the width of each magnetic island within the BALDUR integrated modeling simulations in order to produce a self-consistent local flattening of the plasma profiles. It is found that the main consequence of the NTM magnetic islands is a decrease in the central plasma temperature and total energy. For the DIII-D and JET discharges, it is found that inclusion of the NTMs typically results in a decrease in total energy of the order of 15%. In simulations of ITER, it is found that the saturated magnetic island widths normalized by the plasma minor radius, for the lowest order individual tearing modes, are approximately 24% for the 2/1 mode and 12% for the 3/2 mode. As a result, the ratio of ITER fusion power to heating power (fusion Q) is reduced from $Q=10.6$ in simulations with no NTM islands to $Q=2.6$ in simulations with fully saturated NTM islands. © *2006 American Institute of Physics*. [DOI: 10.1063/1.2205829]

I. INTRODUCTION

Neoclassical tearing modes (NTMs) are instabilities that limit the achievable ratio of plasma pressure to magnetic pressure (plasma β) in tokamak plasmas.[1,2] Unstable neoclassical tearing modes cause the local equilibrium magnetic field of a plasma to reconfigure, trapping helical chains of plasma known as magnetic islands. Magnetic field lines connect the radial inboard and outboard edges of each island, and the thermal diffusivity along a magnetic field line is orders of magnitude larger than the thermal diffusivity across field lines. Consequently, the flow of heat is significantly enhanced across each magnetic island, effectively degrading the plasma energy confinement. Magnetic islands can lead to disruptive instabilities in tokamak experiments.

The time evolution of individual magnetic islands is usually modeled in terms of the extended Rutherford theory.[3–8] The original Rutherford equation[3] was developed to follow the growth of classical tearing modes. In that model, magnetic islands are modeled with singular layers of current and their growth is proportional to Δ', the discontinuity of the logarithmic derivative of the perturbed helical flux. The saturation of the classical tearing mode, which prevents the magnetic islands from growing indefinitely and yields a saturated island width, was first computed by White, Monticello, Rosenbluth, and Waddell.[4] The growth, and subsequent saturation, of the island is modified by the effects of toroidal geometry, neoclassical bootstrap current, polarization current, and electron cyclotron current drive (ECCD) within the island.[5–8] Neoclassical tearing modes, in particular, can be driven by the effect of the bootstrap current, even if the classical tearing mode parameter Δ' is stabilizing. The absence of a pressure gradient and the resulting bootstrap current density inside the island has the effect of suppressing the net current density within the island, which increases the island width. Conversely, using ECCD to increase the current density within the island reduces the island width.

In this paper, however, a different formalism is employed to compute the widths of multiple magnetic islands in their saturated stage.[9] The model used here treats multiple neoclassical tearing modes in arbitrary toroidal geometry with no assumptions made regarding the aspect ratio of the torus or the plasma β. Quasilinear saturated tearing mode equations are obtained by perturbing the static plasma equilibrium force balance equations. This formalism, implemented by the ISLAND module[9] in the National Transport Code Collaboration (NTCC) Module Library,[10] is especially suited to work within an integrated modeling code. Some phenomena in the Rutherford theory, such as the effect of the polarization current, the effect of the electron cyclotron drive, or the incomplete flattening of the pressure profile in smaller magnetic islands, are not implemented in the ISLAND module. Some similarities and differences between

the model considered in this paper and other models are discussed in Sec. II. The derivation of the tearing mode equations for the magnetic islands is summarized in Sec. II A. The distortion in the shape of the magnetic island due to the slope of the radial magnetic perturbation is described in Sec. II B, and the algorithm employed to obtain the saturation width of the magnetic islands is described in Sec. II C.

The ISLAND module is used in the BALDUR[14] predictive integrated modeling code to compute the adverse loss of thermal confinement resulting from the effect of multiple saturated magnetic islands. In order to study the effect of the enhanced transport due to the magnetic islands, simulations of six Joint European Torus (JET),[16] and six DIII-D[15] high confinement (H-mode) discharges from the International Profile Database are carried out for scenarios containing different numbers of magnetic islands. The discharges chosen include three normalized gyroradius scans, two β scans, and a power scan. In addition, BALDUR simulations are carried out for an H-mode scenario in ITER[17,18] in order to investigate the adverse effects of tearing modes on the fusion burn. The adverse effects of magnetic islands in simulations of the JET, DIII-D, and ITER discharges are presented in Secs. III A–III C. In Sec. III D, integrated modeling simulations are used to illustrate the effect of the distortion of the magnetic islands. The effects of saturated neoclassical tearing modes illustrated by their inclusion in integrated modeling simulations are summarized in Sec. IV.

II. MODEL FOR NEOCLASSICAL TEARING MODES

This section contains a description of the quasilinear model used in the ISLAND module to compute the widths of magnetic islands due the neoclassical tearing modes. The theory allows for the simultaneous treatment of multiple magnetic islands, which interact with one another principally through the modification of the background plasma profiles and, to a lesser degree, through harmonic coupling.

Magnetic islands are treated as helical perturbations to the static scalar pressure force balance equilibrium equations. Each magnetic island can be visualized as a flux tube that forms around a magnetic field line in a mode rational surface. In particular, an island forms at each mode rational surface, where the magnetic safety factor q equals the ratio of the poloidal mode number m to the toroidal mode number n. Rotation of the magnetic islands is not considered. The details of the derivation, which involve the increased transport across each magnetic island, the flattening of the plasma profiles within each island, and the coupling of the magnetic islands, can be found in Ref. 9.

The dynamic evolution and growth of magnetic islands, such as in the extended Rutherford equation, is not computed in this work. The neoclassical tearing modes considered in this work are in their saturated stage, i.e., at a stage in which nonlinear effects have detained the growth of the magnetic islands. Heuristically speaking, magnetic islands gradually flatten the plasma profiles as they grow. Eventually, this flattening effect balances the pressure and current density gradients that drive the magnetic islands, and further growth is prevented. In this paper, the nonlinear saturation effects are approximated by completely flattening the plasma profiles across the width of the magnetic island.

It is anticipated that small magnetic islands do not entirely flatten the plasma profiles.[5] This effect, which is not included in this work, is important in the Rutherford theory for determining the threshold widths of islands, but is relatively less important for determining the saturation width of large islands. The saturated widths of the magnetic islands under consideration are all larger than 5% of the plasma radius. Consequently, it is expected that this omission will not cause significant discrepancies between the results of this work and similar computations carried out using the extended Rutherford equation. The variation in the energy confinement as a function of the magnetic island width is discussed in Sec. III E.

From a theoretical point of view, the nonlinear saturation of magnetic islands is not an entirely understood phenomenon.[19,20] In fact, the quasilinear tearing mode theory cannot always reproduce correctly the growth rates and saturation widths of magnetic islands. For instance, disagreement regarding the width of saturated NTM islands in ITER has been found between the extended Rutherford equation and more sophisticated calculations.[21] This finding suggests that inadequacies or oversights could exist in the quasilinear effects usually considered for island saturation. In addition, it has been experimentally observed that even at large island widths the plasma profiles may not become completely flat.[22] This effect is not considered in this paper.

The saturated width of NTM islands is enhanced by the effect of the bootstrap current, especially when the fraction of bootstrap current density with respect to the total current density is high. In the ISLAND module, the effect of the neoclassical bootstrap current is implemented by suppressing the bootstrap current density inside each magnetic island, where the pressure gradient is negligible. The resulting reduction of current density within each island increases the saturated width of the magnetic island.

Magnetic islands located on different magnetic surfaces rotate around the plasma with different frequencies, which are affected by polarization current effects.[23] It has been proposed that the polarization current can be stabilizing or destabilizing depending on the frequency and direction of the rotation of the islands. Additionally, the polarization current is important in the determination of the threshold island width for NTM magnetic islands. By considering a static magnetohydrodynamic model, these effects are not included in this work.

The geometrical effects considered in the ISLAND module result in toroidal couplings between magnetic islands of the same toroidal mode number. This coupling effect allows tearing modes at different radial locations to drive one another. In tokamak experiments, it is observed that the coupling effect between toroidal modes decelerates the rotation of the magnetic islands around the plasma until the islands lock with each other, and also with the vacuum vessel. This phenomenon, which is called mode locking, is affected by the polarization current effects. Mode locking usually leads to the loss of a high confinement mode or to a disruption.

The BALDUR code, with the ISLAND module included,

yields a self-consistent solution for the plasma profiles in the presence of magnetic islands driven by tearing modes. At the present time, it is not practical to implement large nonlinear magnetohydrodynamics (MHD) codes such as NIMROD,[11] M3D,[12] and PIES[13] within integrated modeling codes. Integrated modeling simulations provide a self-consistent approach for treating neoclassical tearing modes together with transport, sources, sinks, sawtooth oscillations, equilibria, and boundary conditions within tokamaks. Nonlinear MHD codes have been utilized to study phenomena such as growth rates for nonlinearly coupled modes, the effects of multiple tearing mode harmonics at the same rational surface, nonaxisymmetric effects, effects of magnetic field line stochasticity, and the dynamic evolution of coupled modes leading to a disruption.[24–26]

A. Tearing mode equations

The derivation of the tearing mode equations starts with the three-dimensional static scalar plasma pressure equilibrium force balance equations, $\mathbf{J}\times\mathbf{B}=\boldsymbol{\nabla}p$, $\boldsymbol{\nabla}\times\mathbf{B}=\mu_0\mathbf{J}$, and $\boldsymbol{\nabla}\cdot\mathbf{B}=0$, which are perturbed about an axisymmetric equilibrium. The perturbed equations are best expressed using Hamada-like flux coordinates (x,θ,ζ). The x coordinate uniquely designates the axisymmetric background equilibrium flux surface, θ is an angle-like variable in the poloidal direction, and ζ is an angle-like variable in the toroidal direction. The Jacobian of the system, given by $\mathcal{J}\equiv(\boldsymbol{\nabla}x\cdot\boldsymbol{\nabla}\theta\times\boldsymbol{\nabla}\zeta)^{-1}=\mathcal{J}(x)$, is chosen to be a surface quantity. The derivation proceeds by expanding in terms of Fourier harmonics the components of the perturbed magnetic field, $\mathbf{B}^1$, and the perturbed current density, $\mathbf{J}^1$, as well as the perturbed pressure, p^1.

The linearization of the plasma equilibrium equations yields two coupled ordinary differential equations [Eqs. (1) and (2)], along with two ancillary algebraic equations [Eqs. (3) and (4)], for each harmonic of the perturbed magnetic field and perturbed pressure,

$$\frac{d}{dx}(-i\mathcal{J}B^{1x}_{mn})=\mathcal{J}(nB^{1\zeta}_{mn}-mB^{1\theta}_{mn}), \tag{1}$$

$$\begin{aligned}(nq-m)B^{0\theta}\left(\frac{d}{dx}B^1_{\theta mn}-imB^1_{xmn}\right)&=\mu_0(nJ^{0\zeta}-mJ^{0\theta})\mathcal{J}B^{1\zeta}_{mn}-i\mathcal{J}B^{1x}_{mn}B^{0\zeta}\frac{d}{dx}\left(\frac{\mu_0J^{0\zeta}}{B^{0\zeta}}\right)\\&\quad+\frac{m\mu_0p^1_{mn}}{B^{0\zeta}}\frac{dB^{0\zeta}}{dx},\end{aligned} \tag{2}$$

$$nB^1_{\zeta mn}=-nB^1_{\theta mn}-i\mathcal{J}B^{1x}_{mn}\left(\frac{\mu_0J^{0\zeta}}{B^{0\zeta}}\right)-\frac{m\mu_0p^1_{mn}}{B^{0\zeta}}, \tag{3}$$

$$(nq-m)B^{0\theta}p^1_{mn}=-iB^{1x}_{mn}\frac{dp^0}{dx}. \tag{4}$$

The main feature of this system of differential equations is that the magnetic islands are driven by the gradients of the background pressure and current density, which appear on the right hand side of Eqs. (2) and (4). Equations (2) and (4) appear to be singular at the mode rational surface, i.e., when $q(x)=m/n$. As shown in Ref. 9, the flattening of the background plasma profiles, $\mu_0J^{0\zeta}/B^{0\zeta}$, $nJ^{0\zeta}-mJ^{0\theta}$, and p^0 within the magnetic islands results in the removal of the singularities in Eqs. (1)–(4). The island widths are adjusted until solutions are found that match the boundary conditions, are continuous, and have continuous first derivatives throughout the plasma.[9] In effect, the saturated magnetic island widths are eigenvalues of the equations. These widths are modified by the island distortion, as described below.

B. Effect of distortion on the width of magnetic islands

The shape of each magnetic island is affected by the radial variation of the perturbed radial magnetic field B^{1x}_{mn}. It will be shown that this effect can increase the saturated widths of the magnetic islands driven by neoclassical tearing modes.

To compute the shape of each magnetic island and the first order distortion effect, a stream function ψ is taken to be constant along magnetic field lines such that $\mathbf{B}\cdot\nabla\psi=0$. The zeroth order and perturbed first order magnetic fields and stream functions can be expressed as

$$\mathbf{B}^0=B^{0\theta}\mathcal{J}\boldsymbol{\nabla}\zeta\times\boldsymbol{\nabla}x+B^{0\zeta}\mathcal{J}\boldsymbol{\nabla}x\times\boldsymbol{\nabla}\theta, \tag{5}$$

$$\begin{aligned}\mathbf{B}^1_{mn}&=B^{1x}_{mn}\mathcal{J}\,\boldsymbol{\nabla}\theta\times\nabla\zeta\sin(m\theta-n\zeta)+(B^{1\theta}_{mn}\mathcal{J}\boldsymbol{\nabla}\zeta\times\boldsymbol{\nabla}x\\&\quad+B^{1\zeta}_{mn}\mathcal{J}\boldsymbol{\nabla}x\times\boldsymbol{\nabla}\theta)\cos(m\theta-n\zeta),\end{aligned} \tag{6}$$

$$\psi(x,\theta,\zeta)=\psi^0(x)+\psi^1_{mn}(x)\cos(m\theta-n\zeta). \tag{7}$$

The substitution of these representations into the condition $\mathbf{B}\cdot\boldsymbol{\nabla}\psi=0$, and the application of the tearing mode, Eq. (1), yields the expression

$$\psi^1_{mn}(x)[nB^{0\zeta}(x)-mB^{0\theta}(x)]=-B^{1x}_{mn}(x)\left(\frac{d\psi^0_{mn}(x)}{dx}\right). \tag{8}$$

The shape of the magnetic island can now be computed with different levels of sophistication by expanding the stream function ψ into a Taylor series of different orders around the mode rational surface $x=x_{mn}$. The zeroth order computation considers the case in which the radial perturbed flux across the magnetic island is a constant. This leads to the well known result

$$W_{mn}=4\sqrt{B^{1x}_{mn}/(nB^{0\theta}\,dq/dx)}\big|_{x=x_{mn}}, \tag{9}$$

where the island width W_{mn} is obtained from the value of the contravariant radial magnetic perturbation, B^{1x}_{mn}, at the mode rational surface x_{mn}. Physically, the island width W_{mn}, which is illustrated in Fig. 1, is half the difference between the half-widths of the unperturbed flux surfaces, passing through the outer and inner edges of the magnetic island.

The distortion of the magnetic island can be included by allowing the radial perturbed flux to vary linearly across the width of the magnetic island. The lowest order Taylor series that satisfies this linear variation yields

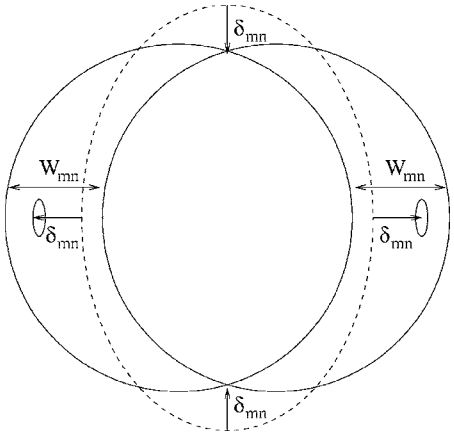

FIG. 1. Distortion of the magnetic island due to the variation of the radial magnetic perturbation. The *X*-point of the island moves inwards, while the *O*-point and the edges of the magnetic island move outward.

$$\psi = \psi^0_{mn}(x_{mn}) - \left(\frac{\psi^1_{mn} n B^{0\theta}}{2iB^{1x}_{mn}} \frac{dq}{dx} \right)_{x=x_{mn}} (x - x_{mn})^2 + \cdots + \left(\psi^1_{mn}(x_{mn}) + \left. \frac{d\psi^1_{mn}}{dx} \right|_{x=x_{mn}} (x - x_{mn}) \right) \cos(m\theta - n\zeta). \tag{10}$$

By requiring that the X point of the magnetic island be an extremum of ψ, it is found that the X point is displaced from the mode rational surface by δ_{mn}, where

$$\delta_{mn} = \left. \frac{\frac{dB^{1x}_{mn}}{dx}}{nB^{0\theta}\frac{dq}{dx}} \right|_{x=x_{mn}}. \tag{11}$$

The O point is displaced by the same quantity δ_{mn}, but in the opposite direction. The value of ψ at the X point can be equated with the value of ψ at the widest part of the island in order to compute the normalized radii of the inner and outer edges of the magnetic island,

$$\left. \begin{matrix} x_{\text{outer}} \\ x_{\text{inner}} \end{matrix} \right\} = (x_{mn} - \delta_{mn}) \pm W_{mn}/2. \tag{12}$$

In this expression, the boundaries of the widest part of the magnetic island are displaced away from the mode rational surface by the quantity $|\delta_{mn}|$. If dB^{1x}_{mn}/dx is negative in the neighborhood of the magnetic island, which it normally is, and dq/dx is positive, then the X point of the magnetic island is displaced toward the magnetic axis and the O point is displaced away from the magnetic axis. Under these conditions, the boundaries at the widest part of the island are displaced away from the magnetic axis and toward the edge of the plasma. This distortion of the magnetic island is illustrated in Fig. 1. The resulting displacement of the local flattening of the pressure and current density profiles enhances the effect of the inboard gradients that drive the magnetic islands. Hence, the saturated widths of the islands usually increase as a result of the distortion. This effect will be illustrated in Sec. III D.

C. Computer algorithm for determining saturated tearing mode island widths

The quasilinear model developed in Ref. 9 can be used iteratively to compute the saturated widths of magnetic islands driven by neoclassical tearing modes. The background axisymmetric current density and pressure profiles outside of the islands, along with the unperturbed flux surface shapes, are taken from the BALDUR predictive integrated modeling code.[14] The precise form of the flattening of the profiles inside each island and corrections to the profiles near each island are computed within the ISLAND module, as described in Ref. 9.

Although linear coupling relations are implemented in the ISLAND module, harmonic coupling effects have not been used in the BALDUR simulations carried out for this paper. More precisely, since only one toroidal harmonic per rational surface is considered, the 4/3, 3/2, and 2/1 islands are not directly coupled. Thus, the integrations associated with each mode are carried out independently with significant gain of computational efficiency relative to the algorithm utilized in Ref. 9.

An adaptive ordinary differential equation solver[27,28] is used to integrate the system of differential equations for the perturbations. Equations (1) and (2) are integrated, for each harmonic, outward from the magnetic axis to the mode rational surface, x_{mn}, as well as inward from the outer boundary to x_{mn}. The conditions at the inner and outer boundaries, $[B^{1x}_{mn}(x_{\text{axis}}), B^1_{\theta mn}(x_{\text{axis}})]$ and $[B^{1x}_{mn}(x_{\text{edge}}), B^1_{\theta mn}(x_{\text{edge}})]$, are chosen to ensure that the radial harmonic $B^{1x}_{mn}(x)$ is continuous throughout the plasma and that the magnitude of $B^{1x}_{mn}(x)$ at the mode rational surface, $x=x_{mn}$, is consistent with the corresponding island width, W_{mn}, given by Eq. (9). This process is then be repeated for any number of harmonics. Since the flattening of each plasma profile within the magnetic island is affected by the distortion of that island, the value of δ_{mn} must be computed by using Eq. (11). Since the value of dB^{1x}_{mn}/dx at the mode rational surface is initially unknown, the displacement δ_{mn} needs to be computed iteratively before the correct magnetic perturbation $B^{1x}_{mn}(x)$ can be computed self-consistently.

The saturated widths of the magnetic islands is obtained by iteratively adjusting W_{mn} until all of the magnetic perturbation harmonics and their first derivatives are continuous throughout the plasma. This requirement is equivalent to the saturation condition $dW_{mn}/dt=0$ in the Rutherford theory. The quasi-linear value of Δ' for each helical harmonic is computed using a quantity proportional to the discontinuity in the derivative of the contra-variant radial magnetic field perturbation near the mode rational surface

$$\Delta'_{mn} \equiv \lim_{\epsilon \to 0} \left(\frac{1}{B^{1x}_{mn}} \frac{dB^{1x}_{mn}}{dx} \right)^{x=x_{mn}+\epsilon}_{x=x_{mn}-\epsilon}. \tag{13}$$

A finite difference form of the equation for each harmonic,

$$\frac{dW_{mn}}{dt} = \frac{x^2_{mn}}{\tau_R} \Delta'_{mn}, \tag{14}$$

similar in form to the Rutherford equation, is used to advance the instantaneous width of the magnetic islands toward

convergence. The resistive timescale τ_R is obtained using the resistivity computed by the BALDUR code. The computation of Δ'_{mn} on the right side of Eq. (14) includes the effects of arbitrary axisymmetric geometry, plasma beta, and the neoclassical bootstrap current. The effect of the rotation of the island, as well as the incomplete flattening of the pressure profile when the magnetic island is small, are absent.

The background pressure and current density profiles are taken from the integrated modeling code that calls the ISLAND module (i.e., from the BALDUR code for the simulations used in this paper). Since the radial grid in the integrated modeling code can be relatively coarse on the scale of the island width, the detailed flattening of the pressure and current density profiles within the islands is computed accurately within the ISLAND module, as described in Ref. 9. If there are multiple harmonics with large amplitude, regions with stochastic magnetic field can form, starting near the X points of the magnetic islands and regions of stochasticity can form in between magnetic islands. This nonlinear effect is not included in the ISLAND module. However, the effect of the stochastic magnetic field near the X point of a magnetic island will be to flatten the profiles more than they would be flattened without the stochasticity. Hence, the result of stochasticity would be to slightly reduce the island widths.

Rotation of the magnetic islands around the plasma is not considered. Consequently, the effect of the magnetic islands upon thermal confinement is that of nonrotating islands with no additional drive through magnetic coupling. Interactions with other tearing modes, and with sawtooth oscillations, are produced only through the axisymmetric modification of the background plasma profiles.

III. MAGNETIC ISLANDS IN TOKAMAK SIMULATIONS

The simulations of JET, DIII-D, and ITER discharges in the high confinement (H-mode) operating regime are described in this section. Integrated modeling simulations included in previous studies[18,29] are repeated, with the addition of neoclassical tearing modes computed using the revised ISLAND module in order to study the impact of magnetic islands driven by NTMs on the plasma temperature profiles and total energy content.

In the BALDUR simulations, anomalous transport is computed using the multimode module,[30] which involves a combination of different theoretical models, while neoclassical transport is computed using the NCLASS module.[31] The plasma magnetic equilibrium is computed self consistently as a function of time using the VMEC2 routine,[32] in which the boundary shape is prescribed as a function of time. A predictive edge model[33] provides the boundary conditions for computing the plasma temperature and density at the top of the edge pedestal. In this edge model, the width of the pedestal is determined by a combination of magnetic and flow shear stabilization of drift modes, while the pedestal pressure gradient is limited by the ballooning mode instability.

In the simulations of ITER, the fusion heating power is determined using nuclear reaction rates together with a Fokker-Planck package to compute the spectrum of fast alpha particles in the plasma. Sawtooth oscillations, which redistribute the fast alpha particles and the central plasma profiles, can have a significant impact on the fusion heating profile. The axisymmetric mixing of plasma profiles after each sawtooth crash is computed using the Kadomtsev model.[34] Experimentally observed sawtooth crash times are used in the simulations of JET and DIII-D. In simulations of ITER, the period of sawtooth oscillations is computed using the Park-Monticello model.[35] The interaction between sawtooth oscillations and NTMs is caused by the modification of the plasma profiles that is produced by both the sawtooth oscillations and the magnetic islands.

To study the effect of the magnetic islands, the simulations are carried out using the protocol used in Refs. 18 and 29. One or more saturated magnetic islands are brought into existence after the discharge has reached quasisteady state. The evolution of the plasma discharge and the magnetic islands is followed until the end of the simulation. Sawtooth crashes are disabled near the end of the simulation in order to avoid the possibility of a sawtooth crash just before the plasma profiles are analyzed. Although large magnetic islands near the edge of the plasma can, in reality, degrade the H-mode pedestal at the edge of the plasma, it is assumed in the simulations that the H-mode pedestal remains at the temperature predicted by the pedestal model.

The simulations are run under the assumption that the islands are initiated with a seed island of sufficient size, and that each island grows to its saturation width. In this work, the effects of saturated islands are efficiently approximated by including fully saturated NTM islands in the simulations, and neglecting the island growth. It is observed in experiments that magnetic islands on different rational surfaces can grow and evolve at different times, and that one of the tearing mode islands can become dominant over others.[36] By considering tearing mode islands that saturate simultaneously, this effect is neglected in the present work.

The saturated width of the neoclassical tearing mode islands is obtained using the ISLAND module that implements the algorithm described in the previous section. After each time step in the integrated modeling code, the widths of the islands are adjusted using Eq. (14). Heat and particle transport are then enhanced across each island to produce flat spots in the temperature, pressure, and current density profiles. Consequently, the presence of magnetic islands alters the evolution of the plasma profiles within the predictive modeling code, which then affects the saturated widths of the magnetic islands in subsequent time steps. In this manner, a nearly self-consistent treatment is obtained.

The following subsections contain the results of these simulations. The effects of saturated magnetic islands on the plasma profiles and stored energy are shown for BALDUR simulations of JET, DIII-D, and ITER discharges in Secs. III A–III C, respectively. Finally, in Sec. III D the effects of the distortion of the magnetic island derived in Sec. II B are examined using simulations of a JET discharge.

TABLE I. Plasma parameters for the JET discharges.

Tokamak	JET	JET	JET	JET	JET	JET
discharge	33131	33140	35156	35171	38407	38415
type	Low ρ_*	High ρ_*	Low ρ_*	High ρ_*	Low β	High β
R (m)	2.94	2.93	2.86	2.88	2.91	2.88
a (m)	0.84	0.85	0.86	0.83	0.86	0.88
κ	1.70	1.56	1.56	1.58	1.60	1.55
δ	0.28	0.20	0.11	0.24	0.16	0.11
B_T (T)	3.06	1.74	2.18	1.09	1.59	1.84
I_p (MA)	2.83	1.61	2.05	1.01	1.47	1.67
$\bar{n}_{e,19}$	7.10	3.65	5.44	2.44	3.05	4.02
Z_{eff}	1.92	1.66	1.25	1.10	2.09	2.06
P_{NB} (MW)	18.0	5.80	8.60	2.91	5.60	15.7
$P_{\text{heat}}/(\bar{n}_{e,19}V)$	0.042	0.027	0.022	0.031	0.027	0.054
$n^{\text{exp}}_{e,19,\text{ped}}$	4.70	2.88	4.60	1.81	2.39	3.02
$T^{\text{exp}}_{e,\text{ped}}$ (keV)	1.47	0.96	2.78	0.61	0.87	1.25
$T^{\text{exp}}_{i,\text{ped}}$ (keV)	1.69	0.96	2.40	0.61	1.04	1.35
$n^{\text{sim}}_{e,19,\text{ped}}$	5.16	2.65	4.34	1.53	2.25	3.24
$T^{\text{sim}}_{\text{ped}}$ (keV)	1.48	1.19	0.72	0.56	1.11	0.88
t_{diag} (s)	15.69	16.50	15.85	25.00	17.40	16.61

A. Effect of the magnetic islands in simulations of the Joint European Torus (JET)

In this section, the saturated tearing mode package is used in the BALDUR code to simulate JET tokamak discharges. The six JET H-mode discharges analyzed consist of two normalized gyroradius ($\rho_\star$) scans and a β scan. In the normalized gyroradius scans, $\rho_\star$ was varied by a factor of 1.6 while holding other dimensionless parameters (magnetic safety factor q, collisionality $\nu_\star$, and plasma β) nearly constant. JET discharges 35156 and 35171 form a matched pair with heating power well above the H-mode power threshold, while JET discharges 33140 and 33131 have heating power near the H-mode threshold. The discharges 38407 and 38415 are from a scan in which β was varied by a factor of 1.5 while holding q, $\nu_\star$, and $\rho_\star$ constant. The plasma parameters and boundary conditions used in the simulations of these JET discharges are listed in Table I.

JET discharge 33131 is used to illustrate the effects of magnetic islands in a low gyroradius discharge. Simulations are carried out with the following scenarios: A simulation with no neoclassical tearing mode islands; a simulation that includes only a 4/3 magnetic island; a simulation that includes only a 3/2 magnetic island; a simulation that includes only a 2/1 magnetic island; a simulation that includes coexisting 3/2 and 2/1 magnetic islands; and a simulation that includes coexisting 4/3, 3/2, and 2/1 islands. Sawtooth oscillations are present along with tearing modes in each simulation.

In the simulation of the JET discharge 33131 that includes only one tearing mode, the average saturated width for the 2/1 magnetic island between $t=15.20$ s and $t=16.00$ s is 15% of the JET minor radius. In this paper, all island widths are normalized by the minor radius (half-width) at the edge of the plasma. It is found that the distortion of the 2/1 island can become large enough to cause the width of the saturated islands to increase noticeably. This phenomenon, which is described in more detail in Sec. III D, also occurs in the simulations of the other JET discharges and ITER. The simulations of discharge 33131 that include only a 3/2 island or a 4/3 island yield an average island width of 8% and 5%, respectively. When 3/2 and 2/1 islands are included in the same simulation, their time averaged widths are 7% and 11%, respectively. Generally, it is found that when additional islands are present, saturated island widths are less than the widths the islands have when other islands are not present. The simulation including the islands associated with the 4/3, 3/2, and 2/1 tearing modes results in time averaged island widths that are 4.5%, 5.5%, and 10% of the plasma minor radius, respectively. In this simulation with three simultaneous islands, it is found that the 4/3 and 3/2 saturated islands overlap with one another.

In Fig. 2 the radial extents of the 4/3, 3/2, and 2/1 islands coexisting in the simulation of discharge 33131 are shown as a function of time. The sawtooth mixing radius is indicated with hollow bars at the time of each crash. The two transient variations in the width of the magnetic islands (primarily in the 4/3 island) observed at $t=15.26$ and at $t=15.81$ s are a consequence of the sawtooth oscillations. In particular, every time a sawtooth crash occurs, the central plasma profiles are flattened within the mixing radius. This causes the current density and pressure profiles to become steeper just outside the mixing region, which then has the effect of enhancing the saturated width of the magnetic islands.

Figure 3 illustrates the electron and ion temperature profiles that result when neoclassical tearing mode islands are treated self-consistently. The simulation profiles for JET discharge 33131 and the experimental profiles (obtained from the International Profile Database and shown with open circles) are plotted at $t=15.69$ s. The small solid dots in Fig.

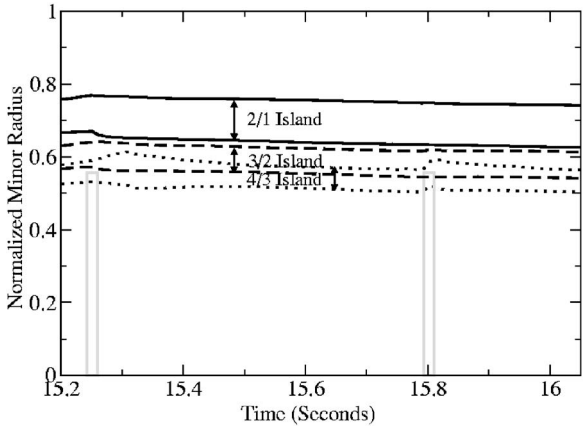

FIG. 2. Inner and outer edges of 2/1, 3/2, and 4/3 magnetic islands as a function of time in a simulation of the JET discharge 33131 with multiple tearing modes coexisting.

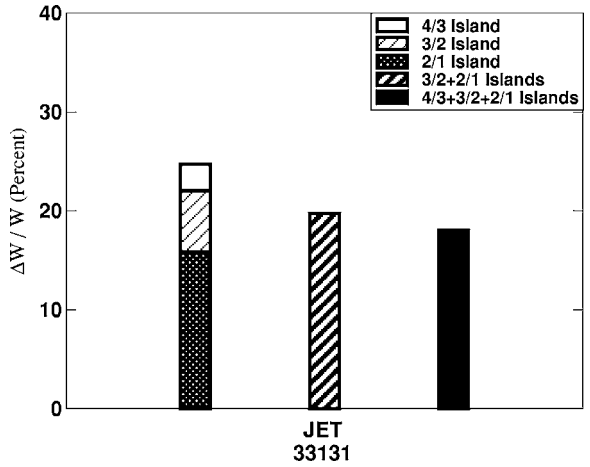

FIG. 4. Total plasma energy loss in simulations of JET discharge 33131 that include different combinations of tearing modes compared to the simulation with no tearing modes.

3 indicate the simulation profiles without magnetic islands present; the thin gray line, the simulation profiles with a 4/3 island; the thin dots, a 3/2 island; the dashed line, a 2/1 island; the dot-dashed line, coexisting 3/2 and 2/1 islands; and the solid black line shows simulation profiles when the three magnetic islands coexist. In simulation profiles for discharges that include multiple tearing modes, the flat spots due to individual magnetic islands are difficult to distinguish, either because the islands overlap with one another or because the distance between the islands is too small. The location and size of each island varies because of the self-consistent evolution of the current density profile resulting from the presence of different numbers of tearing mode islands in each simulation.

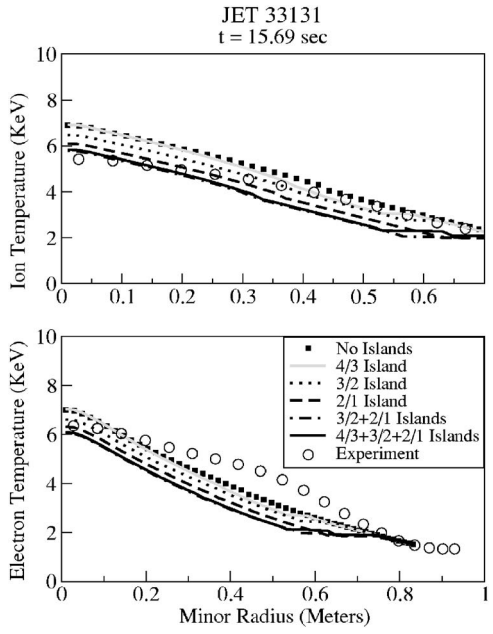

FIG. 3. Electron and ion temperatures profiles in simulations of neoclassical tearing modes in JET discharge 33131 computed at the diagnostic time $t=15.69$ seconds. The flat spots in the profiles correspond to the enhanced transport associated with each magnetic island.

The energy loss as a result of the presence of different combinations of tearing modes in JET discharge 33131 is illustrated in Fig. 4. The left column indicates the energy loss when single islands are present. The middle and right columns indicate the energy loss when two or three islands are present. The decrease in simulated total stored energy for each JET discharge due to the coexistence of the 4/3, 3/2, and 2/1 islands is shown in Fig. 5 for the six JET discharges considered. It is found that the average energy loss is about 18.5%, with a minimum of 13% and a maximum of 22%, for the discharges considered. Usually, the energy loss obtained in simulations of discharges that include islands in addition to the 2/1 island is not much greater than the energy loss when only the 2/1 island is present.

The time averaged widths of magnetic islands, as a percentage of plasma radius, are shown Fig. 6 for the six JET discharges considered. For each discharge, the first column shows the width of each island obtained in simulations in

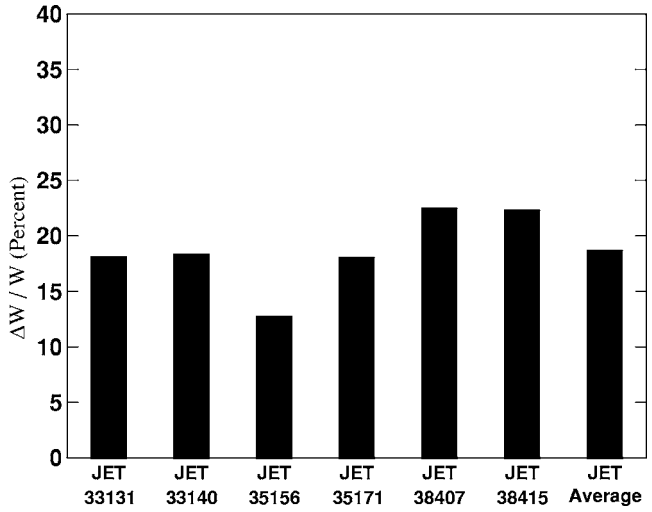

FIG. 5. Decrease in total energy W for simulations of JET discharges in which the 4/3, 3/2, and 2/1 islands coexist compared to the simulations in which neoclassical tearing mode islands are not presented. The comparison is computed at the diagnostic times indicated in Table I.

TABLE II. Plasma parameters for the DIII-D discharges.

Tokamak	DIII-D	DIII-D	DIII-D	DIII-D	DIII-D	DIII-D
discharge	77557	77559	82205	82788	81321	81329
type	Low power	High power	Low ρ_*	High ρ_*	Low n_e	High n_e
R (m)	1.68	1.69	1.68	1.68	1.69	1.70
a (m)	0.60	0.61	0.60	0.59	0.56	0.58
κ	1.85	1.84	1.71	1.67	1.83	1.83
δ	0.33	0.35	0.37	0.35	0.29	0.36
B_T (T)	2.00	2.00	1.81	0.95	1.98	1.97
I_p (MA)	1.00	1.00	1.34	0.66	0.99	1.00
$\bar{n}_{e,19}$	4.88	5.02	5.34	2.86	2.94	5.35
Z_{eff}	1.68	2.21	2.13	1.94	2.42	1.65
P_{NB} (MW)	4.73	13.23	5.86	3.25	3.49	8.34
$P_{\text{heat}}/(\bar{n}_{e,19}V)$	0.047	0.123	0.058	0.063	0.065	0.083
$n^{\text{exp}}_{e,19,\text{ped}}$	3.22	3.38	3.93	2.28	2.13	3.38
$T^{\text{exp}}_{\text{e,ped}}$ (keV)	0.55	0.57	0.83	0.48	0.88	0.44
$T^{\text{exp}}_{i,\text{ped}}$ (keV)	0.44	0.27	0.95	0.57	1.32	0.55
$n^{\text{sim}}_{e,19,\text{ped}}$	3.60	3.67	3.96	2.06	2.21	3.84
$T^{\text{sim}}_{\text{ped}}$ (keV)	0.40	0.39	0.79	0.51	0.91	0.47
t_{diag} (s)	2.70	2.70	3.66	3.54	3.90	3.80

which only one island is present at a time. The second column shows the combined widths of the 3/2 and 2/1 islands obtained in a simulation in which these two islands are present simultaneously. The third column indicates the combined widths when the 4/3, 3/2, and 2/1 islands coexist. It is found that in the simulations in which only the 2/1 island is present, the width of the 2/1 island is greater than the width of the 2/1 island in simulations in which additional islands are present. A similar effect is also observed for the 3/2 island. This decrease in the width of an island when multiple islands are present is a consequence of the interaction between the coexisting magnetic islands. The flat spots produced by islands closer to the magnetic axis have the effect of reducing the driving force available for the islands farther away from the magnetic axis.

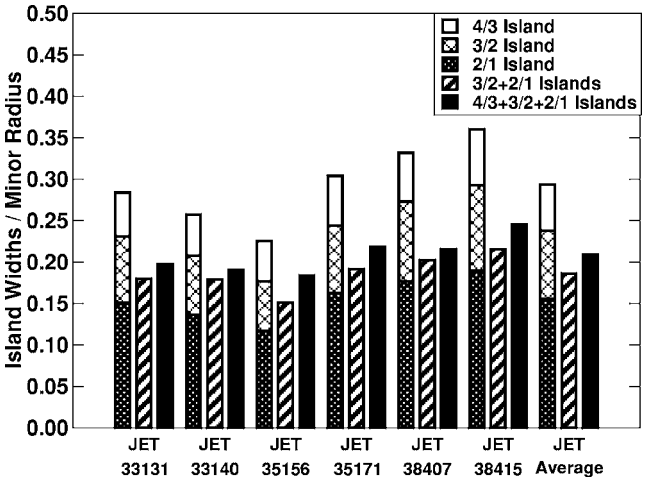

FIG. 6. Time averaged widths of magnetic islands in simulations of JET discharges. For each discharge, the first (left) column shows the width of the 4/3, 3/2, and 2/1 islands in simulations that included only one island, the second column shows the width of the neoclassical tearing mode islands when the 3/2 and 2/1 islands coexist, and the third column shows the width when the 4/3, 3/2, and 2/1 islands coexist.

B. Effect of the magnetic islands in simulations of DIII-D

The six DIII-D H-mode discharges that are simulated include a power scan, a β scan, and a gyroradius ($\rho_\star$) scan. In DIII-D discharges 77557 and 77559, the heating power was varied while the plasma density was held constant. DIII-D discharges 82 205 and 82 788, which result from a gyroradius scan, have the same plasma shape, β, and collisionality as the projected ITER design. Discharges 81 321 and 81 329 are from a density scan. The plasma parameters and boundary conditions used in the simulations of these DIII-D discharges are listed in Table II.

The results of simulations of discharge 77559 with tearing modes present illustrate the effect of tearing modes in a DIII-D high power discharge. For this discharge, it was found that the 4/3, 3/2, and 2/1 saturated magnetic islands are driven by neoclassical tearing modes. The simulations carried out include the following scenarios: No neoclassical tearing mode islands present; only a 2/1 magnetic island; only a 3/2 island; only a 4/3 island; coexisting 2/1 and 3/2 islands; and coexisting 4/3, 3/2, and 2/1 islands. The neoclassical tearing modes in this discharge are shown at a time that is in between sawtooth crashes.

In simulations that include only one tearing mode it is found that the average saturated width for the 2/1 island, between $t=2.65$ s and $t=2.70$ s, is 18% of the minor DIII-D radius; for the 3/2 island, 11%; and for the 4/3 island, 8%. The time averaged width of coexisting 2/1 and 3/2 islands is 28% of the minor DIII-D radius, while the time averaged width when the 4/3, 3/2, and 2/1 islands coexist is 37%. In

the latter simulation the width of the 4/3 island is 8%, the width of the 3/2 island is 11%, and the width of the 2/1 island is 18%.

The effects of magnetic islands on the electron and ion temperature profiles are shown in Fig. 7. The simulation profiles for DIII-D discharge 77559 and the experimental profiles (obtained from the International Profile Database, shown with open circles) are plotted at $t=2.70$ s. The solid dots indicate the simulation profiles without magnetic islands present; the thin gray line, the simulation profiles with a 4/3 island; the thin dots, a 3/2 island; the dashed line, a 2/1 island; the dot-dashed line, coexisting 3/2 and 2/1 islands; and the solid black line shows simulation profiles in which three magnetic islands coexist. The location and size of each island varies because of the self-consistent evolution of the current density profile resulting from the presence of different numbers of tearing mode islands in each simulation.

The time averaged widths of the magnetic islands in simulations of DIII-D discharges with tearing modes present are shown in Fig. 8. The total width of the islands in simulations in which the 2/1, 3/2, and 4/3 coexist ranges from 17% for discharge 77557 to 36% for discharge 77559, and the average total width for the 6 DIII-D discharges considered is 22%. The decrease in the simulated total stored energy for each DIII-D discharge due to the coexistence of the 4/3, 3/2, and 2/1 islands is shown in Fig. 9. It is found that the average energy loss is about 13%, with a minimum of 8% for DIII-D discharge 77557 and a maximum of 18% for DIII-D discharge 77559.

C. Effect of the magnetic islands in simulations of ITER

Simulations of a conventional H-mode discharge in ITER[18] were carried out using the same protocol that was used above in the simulations of JET and DIII-D. The results

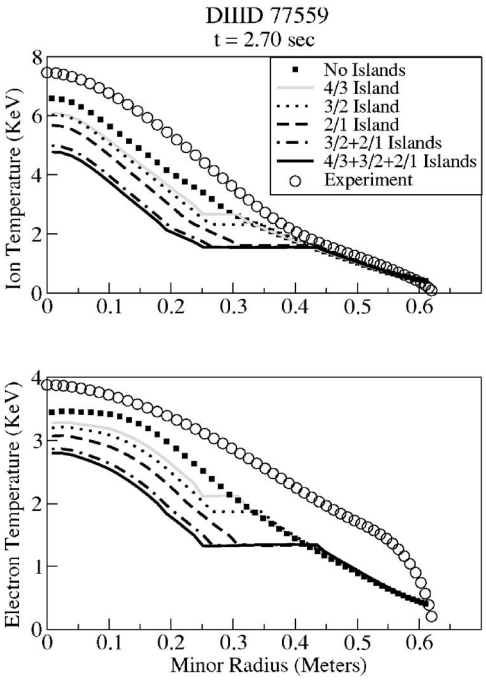

FIG. 7. Electron and ion temperatures profiles in simulations of neoclassical tearing modes in DIII-D discharge 77559. The flat spots in the profiles correspond to the enhanced transport due to each magnetic island.

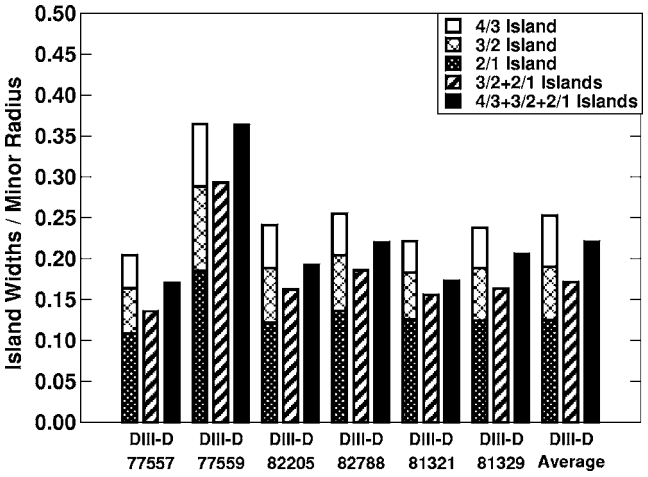

FIG. 8. Time averaged widths of magnetic islands in simulations of DIII-D discharges. For each discharge, the left column shows the width of the 4/3, 3/2, and 2/1 islands in simulations that included only one tearing mode, the center column shows the combined width of the 3/2 and 2/1 islands, and the right column shows the combined width of the 4/3, 3/2, and 2/1 islands.

of ITER simulations that were carried out with no islands are compared with results of simulations with various combinations of islands, including a simulation of the ITER discharge with only the 3/2 island present; a simulation with only the 2/1 island present; a simulation in which the 3/2 and the 2/1 islands coexist; and a simulation in which the 3/2, the 2/1, and the 4/3 islands coexist. As previously noted, feedback stabilization of the islands, for example, by current drive, is not included. Also, it is assumed that all the islands that are considered in each simulation are seeded and grow to their saturated widths. Hence, these simulations describe the maximum reduction of confinement associated with NTMs and the simulations are intended to illustrate the importance of limiting the growth of NTMs.

The inner and outer edges of a 2/1 island, normalized by the minor plasma radius, are shown as a function of time in Fig. 10. The sawtooth mixing region is indicated at the time of each crash with a hollow bar. The simulation yields a time

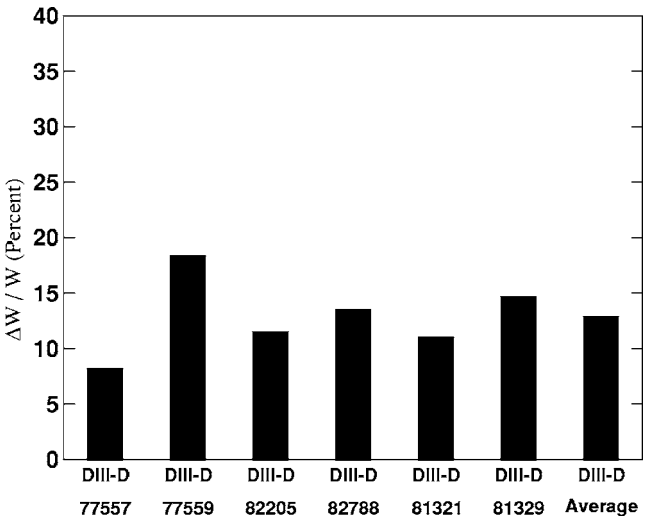

FIG. 9. Decrease in total energy for simulations of six DIII-D dishcarges that include the effect of multiple tearing modes.

averaged saturated width of the 2/1 island that is 24.5% of the ITER minor plasma radius. The simulation that includes only a 3/2 magnetic island yields a time averaged width of 12.5 %. In Fig. 11 the radial extents of the 4/3, 3/2, and 2/1 magnetic islands are shown for a simulation of an ITER plasma in which these three islands coexist. The time averaged fraction of the plasma covered by the three magnetic islands is approximately 28% of the minor plasma radius, and it is found that the saturated magnetic islands overlap one another. The overlap of magnetic islands resulting in catastrophic ergodization of the equilibrium magnetic field lines has been considered as a possible trigger for disruptive instabilities.

The variations in the width of the magnetic islands observed in Figs. 10 and 11 are a consequence of the sawtooth oscillations. More specifically, each sawtooth crash causes the pressure and current density gradients to be steepened just outside the mixing region, affecting the saturated width of the magnetic islands. In the Park-Monticello model, which is used to trigger the sawtooth crashes in the simulations, the period of the sawtooth oscillation decreases with lower central electron temperature. Hence, once the central temperature is sufficiently reduced due to the presence of the magnetic islands, the sawtooth oscillations occur much more frequently and their amplitude decreases. In a simulation without magnetic islands, for instance, only three sawtooth crashes were observed in the time interval shown in Figs. 10 and 11 and the mixing radii were significantly less than the values obtained in the simulations that included tearing mode islands. Changes in the shape of the current density profile cause changes in the sawtooth mixing radius.

The effects produced by the magnetic islands on the ITER ion temperature as a function of the minor radius, in simulations in which the islands are treated self-consistently, are shown in Fig. 12. The profiles are plotted at the conclusion of the ITER simulation (t=300 s). The solid dots indicate the result obtained in a simulation without magnetic islands; the thin dots, a simulation with only a 3/2 magnetic island present; the dashed line, a simulation with only a 2/1 magnetic island present; the dot-dashed line, a simulation with both the 3/2 and 2/1 islands present; and the solid line indicates the results obtained in the simulation where the 4/3, 3/2, and 2/1 magnetic islands coexist. The increased transport due to the tearing modes results in flat spots in the temperature profiles, although, in the simulation where the three islands coexist, the small distance between the 4/3 and the 3/2 magnetic island makes it difficult to distinguish their individual flat spots.

The flat spot due the 2/1 magnetic island is visibly smaller in simulations with multiple tearing mode islands compared with the flat spot produced by a 2/1 island when other islands are not present. This is a consequence of the interaction between the coexisting magnetic islands. Also, the positions of the flat spots vary due to the self-consistent evolution of the current density profile in each simulation caused by the presence of a different number of magnetic islands.

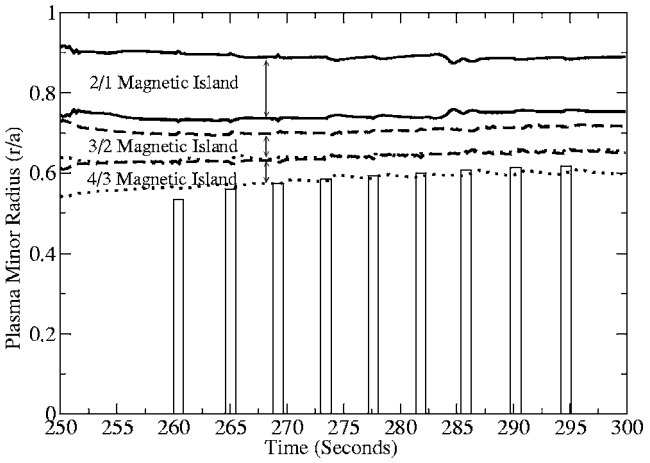

FIG. 11. Inner and outer edges of 4/3, 3/2, and 2/1 magnetic islands in a simulation of ITER as a function of time. The sawtooth mixing radii are indicated by hollow bars.

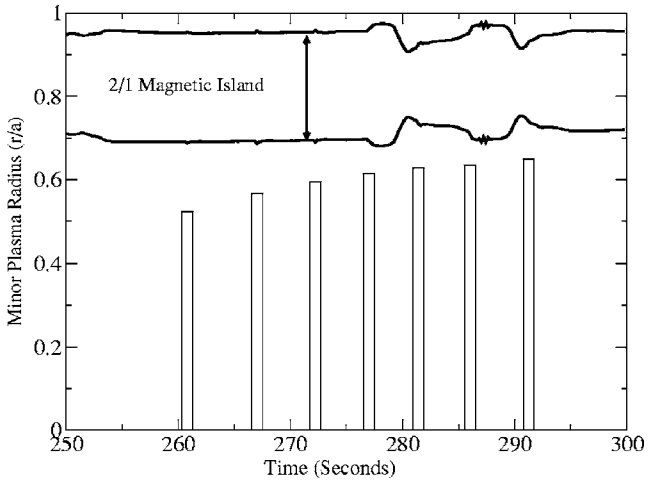

FIG. 10. Inner and outer edges of a 2/1 magnetic island in ITER as function of time. The sawtooth mixing radii are indicated by hollow bars.

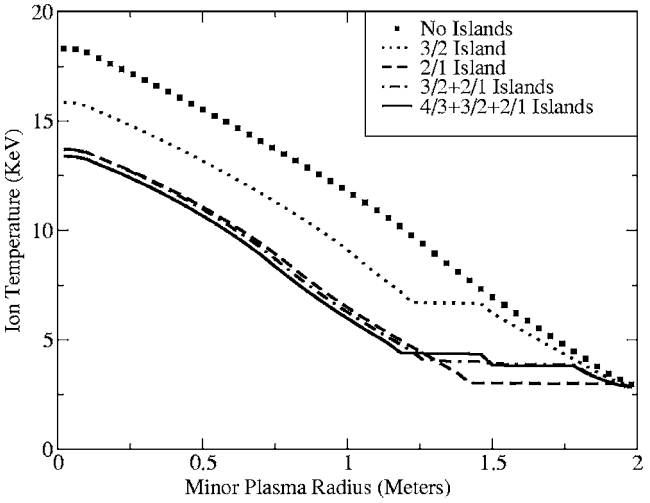

FIG. 12. Electron and ion temperature profiles for simulations of neoclassical tearing modes in ITER. The flat spots observed correspond to the enhanced transport caused by each magnetic island.

TABLE III. ITER simulations carried out with no islands and with various island combinations. Results are presented for the fraction of the plasma radius occupied by the islands, the central plasma temperature in keV, the fusion Q, and the plasma β.

Scenario	$\frac{W_{3/2}}{a}$	$\frac{W_{2/1}}{a}$	$\frac{W_{4/3}}{a}$	$T_{i,0}$	Q	β
No islands	—	—	—	18.3	10.6	2.5
3/2	0.13	—	—	15.8	6.2	2.0
2/1	—	0.25	—	13.7	2.8	1.4
3/2 and 2/1	0.10	0.14	—	13.6	2.6	1.5
3/2, 2/1, and 4/3	0.07	0.15	0.06	13.3	2.4	1.4

Parameters obtained at the end of the ITER simulations (at 300 s) are listed in Table III for the time averaged widths of the magnetic islands normalized by the minor plasma radius, W_{mn}/a, the central ion temperature in keV, the predicted ratio of fusion power to heating power (fusion Q), and the normalized plasma β. The enhanced transport associated with the presence of saturated magnetic islands results a degradation of plasma confinement. As a consequence, there is a decrease in the central ion temperature and a substantial reduction in the fusion yield. It can be seen from the simulation results presented in Table III that the presence of saturated tearing modes can result in a decrease in fusion Q from 10.6 to a value below 3. Also, the simulations illustrate that the combined effect of multiple saturated tearing mode islands on plasma confinement is similar to the effect on confinement that results from a solitary 2/1 island. It is clear that feedback stabilization is probably needed to prevent NTM islands from growing to these large widths in ITER.

D. Effect of the distortion of the magnetic island

The displacement of the local flattening of the pressure and current density profiles caused by the distortion of the magnetic island has the effect of enhancing the inboard gradients that drive the magnetic islands. Consequently, the distortion of the island can enhance the growth of the magnetic island and increase its saturated width.

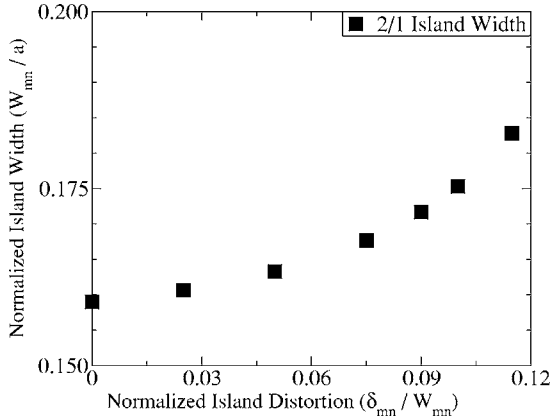

FIG. 13. Saturated width of the 2/1 magnetic island, normalized by the minor plasma radius, as a function of island distortion δ_{mn} normalized by island width in a simulation of JET discharge 38407.

In the simulations of DIII-D discharges, the displacement δ_{mn}, given in Eq. (11), due to the distortion of the islands remains small so that the effect of island distortion is negligible. However, in the simulations of the JET discharges, the outboard shift of the island, associated with the displacement of the X point, can be more than 10% of the island width. In Fig. 13, the normalized width of the 2/1 island is plotted as a function of the island displacement for JET discharge 38407. In the simulation of this discharge with only the 2/1 island present, the displacement of the island is 12% of the island width and the width of the 2/1 saturated island is 18.4% of the plasma radius. However, if the effect of the X-point displacement is omitted, the saturated width of the 2/1 magnetic island is found to be 16% of the plasma radius.

In Fig. 14, the dependence of Δ' [Eq. (13)] on the normalized island width W_{mn}/a is illustrated for the cases with and without the effect of the distortion of the island. The value of the saturated normalized island width is given by the value of W_{mn}/a associated with $\Delta'=0$. Thus, it is observed that a larger saturated island width results when the effect of distortion is taken into account.

E. Energy loss as a function of island width

This section contains a summary of the adverse effects of neoclassical tearing mode islands on thermal confinement, which is illustrated by showing the energy loss predicted by

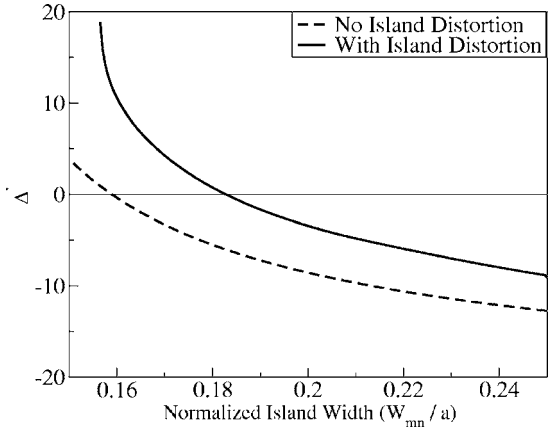

FIG. 14. Illustration of the dependence of Δ' on W/a with and without island distortion for the 2/1 island considered in Fig. 13. The value of the saturated normalized island width is given by the value of W/a associated with $\Delta'=0$.

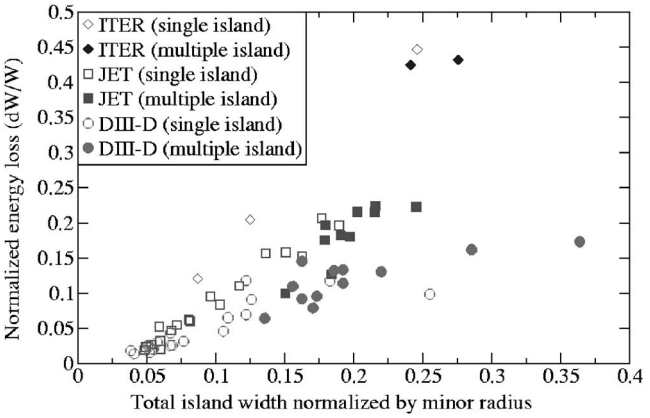

FIG. 15. The total normalized energy loss is shown as a function of total island width, normalized by the minor radius, for simulations of six DIII-D discharges, six JET discharges, and ITER. In each case, five simulation scenarios were carried out, each one containing either one or multiple concurrent NTM islands. The open symbols show simulations that include only a single NTM island, while the filled symbols show simulations that include multiple concurrent islands.

BALDUR simulations as a function of the total island width predicted by the ISLAND module. The normalized energy loss, $\Delta W/W$, is shown in Fig. 15 as a function of the island width for DIII-D, JET, and ITER simulations that include either single or multiple concurrent magnetic islands. As expected, the energy loss increases with an increasing total island width.

It is observed that, despite moderate scatter, the computed energy loss is approximately proportional to the island width. Discharges of DIII-D yield a proportionality constant of 0.55, discharges of JET a proportionality constant of 1.11, and discharges of ITER a proportionality constant of 1.79. The increase in energy loss, especially in DIII-D and JET, is slower for simulations that include more than one concurrent island. Additionally, the two simulations of ITER that included multiple islands resulted in less energy loss than a simulation that included only a 2/1 island. This finding suggests that there could be a saturation effect regarding the energy loss, i.e., that once a certain island width is reached, further energy loss is decelerated. In ITER simulations, quite plausibly, the energy loss differential is larger than in JET or DIII-D discharges because lower central ion temperatures result in decreased fusion yield and, consequently, in diminished alpha particle heating. Hence, a magnetic island of the same given width will have more effect upon an ITER discharge than, let us say, a JET or DIII-D discharge.

IV. CONCLUSIONS

In this paper, the NTCC ISLAND module is improved and is used to compute the effect of saturated neoclassical tearing modes in predictive integrated simulations of DIII-D, JET, and ITER discharges. The simulations are carried out using a protocol that combines predictive models for the edge and for the core of the plasma in the BALDUR code. Plasma magnetic equilibrium surface shapes, sinks and sources of heat and particles, the current profile, and the effect of the sawtooth oscillations are all computed self-consistently. The model for the neoclassical tearing mode islands used in the BALDUR simulations is valid for axisymmetric toroidal plasmas of arbitrary aspect ratio, plasma cross-sectional shape, and plasma β, including the effect of the bootstrap current. The islands produce flat spots in the plasma pressure and current density profiles. These profiles are then used in subsequent time steps to compute the widths of the saturated magnetic islands. The enhanced transport associated with the islands can result in a decrease of the central ion and electron temperatures, and consequently in a decrease of the total plasma energy.

In carrying out the simulations, it is assumed that island seeds of sufficient size exist and the islands grow to their saturated widths. Also, although, in reality, large magnetic islands near the plasma edge could degrade the H-mode pedestal, or terminate the discharge, it is assumed in the simulations that the temperature at the top of the H-mode pedestal remains constant. To avoid this assumption a more advanced, dynamic model for the plasma edge that includes the interaction with the magnetic islands is required. Finally, the simulations carried out do not account for the rotation of the islands or incorporate possible feedback stabilization mechanisms.

Simulations with magnetic islands absent and with various combinations of magnetic islands are carried out for six JET discharges and six DIII-D discharges. In the JET simulations that include only a single island, the average width of the 3/2 island is 9% and of the 2/1 island, 17%; whereas in simulations of DIII-D discharges with a single island, it is found that the average width of the 3/2 island is 7% and of the 2/1 island 13%. The average decrease of total plasma energy caused by magnetic islands when the 4/3, 3/2, and 2/1 islands coexist is 21% in the JET simulations and 12% in the DIII-D simulations. In most of the cases studied, it is found that the addition of an inboard island results in only a slight additional decrease in total plasma energy.

The distortion of a magnetic island due to the variation of the radial magnetic perturbation across the width of the island is derived and incorporated in the simulations. A nonlinear iteration is implemented in the algorithm used to compute the width of the saturated magnetic islands in order to enforce the condition that the radial magnetic perturbation and the distortion of the island are treated self-consistently. The distortion causes the edges of the widest part of the magnetic island to be displaced away from the magnetic axis, enhancing the effects of the inboard pressure and current density gradients that drive the tearing modes. Consequently, the effect of magnetic island distortion results in an increase of the saturated widths of the islands.

Finally, a worst case scenario regarding the possible consequences of neoclassical tearing modes in ITER has been examined. The simulations of ITER indicate that if NTM islands are allowed to grow to their full saturated widths, their effect is devastating. In the case of simulations including only one NTM, the widths of the saturated magnetic island computed in this work are significant and in agreement with previous estimates. In Refs. 2 and 38, estimates for the saturated width of the 2/1 magnetic island range between 58 and 70 cm, in reasonable agreement with the

results presented here. Values for both the 3/2 and the 2/1 magnetic islands are also in good agreement with estimates presented by Hegna at the 2002 Snowmass Fusion Forum. It should be noted that the Hegna results were obtained using a formalism that is rather different from the one used in this paper.

Some important effects are not included in these simulations. For instance, experimental observation suggests that low order magnetic islands can destroy the H-mode pedestal at the edge of the plasma, causing termination of the high confinement regime or even disrupting the discharge. In the simulations presented here, it is assumed that the H-mode pedestal remains unaffected by NTM islands. The large islands obtained in these simulations make it plausible that the pedestal could be degraded. To evaluate this effect, it would be necessary to have a better theoretical understanding of the interaction between the islands and the pedestal, and to have a more sophisticated plasma edge model that can dynamically interact with the magnetic islands. In addition, an accurate, physically correct triggering mechanism for the threshold of required magnetic island seeds needs to be developed. Such a model would shed some light on what the real consequences of neoclassical tearing modes will be for ITER and for other burning plasma experiments. In any event, both the analytical theory and the scaling of experimental data suggest that the width of the threshold islands for ITER will be small.

In view of the results presented here, a mechanism to control the growth of the tearing modes might be necessary for the successful operation of ITER. In that respect, steady progress has been made at DIII-D, ASDEX-U, and JT60-U with regard to controlling NTMs using Electron Cyclotron Current Drive (ECCD).[37–39] For instance, the full suppression of magnetic islands has been achieved in some cases, with the added benefit that the plasma β can be increased above the limiting instability threshold. Recent computational studies[8] have shown that a combined power of 25 MW might be required to control the 3/2 and 2/1 modes in ITER. The design of ITER includes 20 MW of ECCD, with the option of an additional 20 MW upgrade.

ACKNOWLEDGMENTS

We thank Canh Nguyen and Alexei Pankin for their help with the ISLAND module, as well as Rob La Haye and Chris Hegna for their insight and discussions about neoclassical tearing modes.

This work was supported by the U.S. Department of Energy under Contract No. DE-FG02-92-ER-5414.

[1] R. J. La Haye, R. J. Buttery, S. Guenter, G. T. A. Huysmans *et al.*, Phys. Plasmas **7**, 3349 (2000).
[2] O. Sauter, R. J. La Haye, Z. Chang *et al.*, Phys. Plasmas **4**, 1654 (1997).
[3] P. Rutherford, Phys. Fluids **16**, 1903 (1973).
[4] R. B. White, D. A. Monticello, M. N. Rosenbluth, and B. V. Waddell, Phys. Fluids **20**, 800 (1977).
[5] R. Fitzpatrick, Phys. Plasmas **2**, 825 (1995).
[6] A. Glasser, J. Green, and J. Johnson, Phys. Fluids **18**, 875 (1975).
[7] H. Wilson, J. Connor, R. Hastie, and C. Hegna, Phys. Plasmas **3**, 248 (1996).
[8] N. Hayashi, T. Ozeki, K. Hamamatsu, and T. Takizuka, Nucl. Fusion **44**, 477 (2004).
[9] C. N. Nguyen, G. Bateman, and A. H. Kritz, Phys. Plasmas **11**, 3460 (2004).
[10] A. H. Kritz, G. Bateman, J. Kinsey, A. Pankin, T. Onjun *et al.*, Comput. Phys. Commun. **164**, 108 (2004).
[11] C. R. Sovinec, A. H. Glasser, D. C. Barnes *et al.*, J. Comput. Phys. **195**, 355 (2004).
[12] W. Park, E. V. Belova, G. Y. Fu *et al.*, Phys. Plasmas **6**, 1796 (1999).
[13] A. Reiman and N. Pomphrey, J. Comput. Phys. **94**, 225 (1991).
[14] C. E. Singer, D. E. Post, D. R. Mikkelson *et al.*, Comput. Phys. Commun. **49**, 275 (1988).
[15] J. Luxon, Nucl. Fusion **42**, 614 (2002).
[16] P. H. Rebut, R. J. Bickerton, and B. E. Keen, Nucl. Fusion **25**, 1011 (1985).
[17] R. Aymar, P. Barabaschi, and Y. Shimomura, Plasma Phys. Controlled Fusion **44**, 519 (2002).
[18] G. Bateman, T. Onjun, and A. H. Kritz, Plasma Phys. Controlled Fusion **45**, 1939 (2003).
[19] R. J. Hastie, F. Militello, and F. Porcelli, Phys. Rev. Lett. **95**, 065001 (2005).
[20] Q. Yu, S. Günter, and K. Lackner, Phys. Plasmas **11**, 140 (2004).
[21] H. Lütjens and J.-F. Luciani, Phys. Plasmas **12**, 080703 (2005).
[22] A. M. M. Fonseca, V. S. Tsypin, R. M. O. Galvão *et al.*, Phys. Plasmas **12**, 052501 (2005).
[23] J. W. Connor, F. L. Waelbroeck, and H. R. Wilson, Phys. Plasmas **8**, 2835 (2001).
[24] L. E. Sugiyama, W. Park, H. R. Strauss *et al.*, Nucl. Fusion **41**, 739 (2001).
[25] S. E. Kruger, D. D. Schnack, and C. R. Sovinec, Phys. Plasmas **12**, 056113 (2005).
[26] A. L. Rosenberg, D. A. Gates, A. Pletzer *et al.*, Phys. Plasmas **9**, 4567 (2002).
[27] L. F. Shampine and M. K. Gordon, *Computer Simulation of Ordinary Differential Equations: The Initial Value Problem* (Freeman, San Francisco, 1991).
[28] See National Technical Information Service Document No. N94-35259/8, K. Radhakrishnan and A. C. Hindmarsh, *Description and Use of LSODE, the Livermore Solver for Ordinary Differential Equations*. Copies can be ordered from the National Technical Information Service, Springfield VA 22161.
[29] G. Bateman, M. A. Bandrés, T. Onjun, A. H. Kritz, and A. Pankin, Phys. Plasmas **10**, 4358 (2003).
[30] G. Bateman, A. H. Kritz, J. E. Kinsey, A. J. Redd, and J. Weiland, Phys. Plasmas **5**, 2207 (1998).
[31] W. A. Houlberg, K. C. Shaing, S. P. Hirshman, and M. C. Zarnstorff, Phys. Plasmas **4**, 3230 (1997).
[32] S. P. Hirshman and J. C. Whitson, Phys. Fluids **26**, 3553 (1983).
[33] T. Onjun, G. Bateman, A. H. Kritz, and G. Hammet, Phys. Plasmas **9**, 5018 (2002).
[34] B. B. Kadomtsev, Sov. J. Plasma Phys. **1**, 390 (1975).
[35] W. Park and D. Monticello, Nucl. Fusion **30**, 2413 (1990).
[36] Q. Yu, S. Günter, K. Lackner *et al.*, Nucl. Fusion **40**, 2031 (2000).
[37] R. Prater, R. J. La Haye, J. Lohr, T. C. Luce *et al.*, Nucl. Fusion **43**, 1128 (2003).
[38] H. Zohm, G. Gantenbeina, G. Giruzzib, S. Günter *et al.*, Nucl. Fusion **39**, 577 (1999).
[39] A. Isayama, Y Kamada, S Ide, K Hamamatsu *et al.*, Plasma Phys. Controlled Fusion **42**, L37 (2001).